

A repeat sequence domain of the ring-exported protein-1 of *Plasmodium falciparum* controls export machinery architecture and virulence protein trafficking

Emma McHugh,¹ Steven Batinovic,¹ Eric Hanssen,^{1,2} Paul J. McMillan,^{1,3} Shannon Kenny,¹ Michael D. W. Griffin,¹ Simon Crawford,⁴ Katharine R. Trenholme,⁵ Donald L. Gardiner,⁵ Matthew W. A. Dixon,^{1†} and Leann Tilley^{1*†}

¹Department of Biochemistry and Molecular Biology, University of Melbourne, Melbourne, Australia.

²Advanced Microscopy Facility, University of Melbourne, Parkville, VIC 3010, Australia.

³Biological Optical Microscopy Platform, Bio21 Molecular Science and Biotechnology Institute, Parkville, VIC 3010, Australia.

⁴School of BioSciences, University of Melbourne, Parkville, VIC 3010, Australia.

⁵Infectious Diseases Division, Queensland Institute of Medical Research, 300 Herston Rd, Herston, QLD 4006, Australia.

Summary

The malaria parasite *Plasmodium falciparum* dramatically remodels its host red blood cell to enhance its own survival, using a secretory membrane system that it establishes outside its own cell. Cisternal organelles, called Maurer's clefts, act as a staging point for the forward trafficking of virulence proteins to the red blood cell (RBC) membrane. The Ring-EXported Protein-1 (REX1) is a Maurer's cleft resident protein. We show that inducible knockdown of REX1 causes stacking of Maurer's cleft cisternae without disrupting the organization of the knob-associated histidine-rich protein at the RBC membrane. Genetic dissection of the REX1 sequence shows that loss of a repeat sequence domain results in the formation of giant Maurer's cleft stacks. The stacked Maurer's clefts are decorated with tether-like structures and retain the ability to dock onto the RBC membrane skeleton. The REX1 mutant parasites show deficient export of the major virulence protein, PfEMP1, to the red blood

cell surface and markedly reduced binding to the endothelial cell receptor, CD36. REX1 is predicted to form a largely α -helical structure, with a repetitive charge pattern in the repeat sequence domain, providing potential insights into the role of REX1 in Maurer's cleft sculpting.

Introduction

Despite enormous efforts, malaria remains a disease of global significance. Annually about 600 000 deaths are attributed to infection with *Plasmodium falciparum* (Murray *et al.*, 2012; World Health Organization, 2014). The particular virulence of *P. falciparum* is due, in part, to the cytoadherence of infected red blood cells (RBCs) to the walls of post-venule capillaries. Mediated by a protein called *P. falciparum* erythrocyte membrane protein-1 (PfEMP1) (Baruch *et al.*, 1995; Scherf *et al.*, 2008), cytoadherence enables *P. falciparum* to avoid splenic clearance, thus permitting a more rapid multiplication rate. An exacerbated inflammatory response to the sequestered parasites is involved in precipitating severe complications, such as coma and underweight births (Beeson *et al.*, 2001; Turner *et al.*, 2013; White *et al.*, 2014).

Because mature human RBCs lack the machinery for protein synthesis and trafficking, export of *Plasmodium* virulence proteins requires the assembly of a parasite-derived exomembrane system in the host RBC cytoplasm. For example, PfEMP1, an integral membrane protein, is secreted through the parasite's endomembrane system and exported across the parasitophorous vacuole membrane (PVM) in which the parasite resides (Maier *et al.*, 2009). It is trafficked to compartments known as the Maurer's clefts, and then transferred to the RBC membrane, where it is assembled into knobs (Voigt *et al.*, 2000). Despite its importance, much remains unclear about the trafficking, sorting and fusion machinery that mediates delivery of PfEMP1 to the RBC surface.

The term Maurer's *cleft* is, in fact, a misnomer as these parasite-derived structures are flattened cisternae, with no direct opening onto the RBC surface. In the 3D7 strain, they number ~ 15 per cell and are roughly disc-shaped,

Accepted 23 August, 2015. *For correspondence. E-mail ltilley@unimelb.edu.au; Tel. (+61) 3 8344 2321; Fax (+61) 3 8348 1421. †These authors had equal contribution.

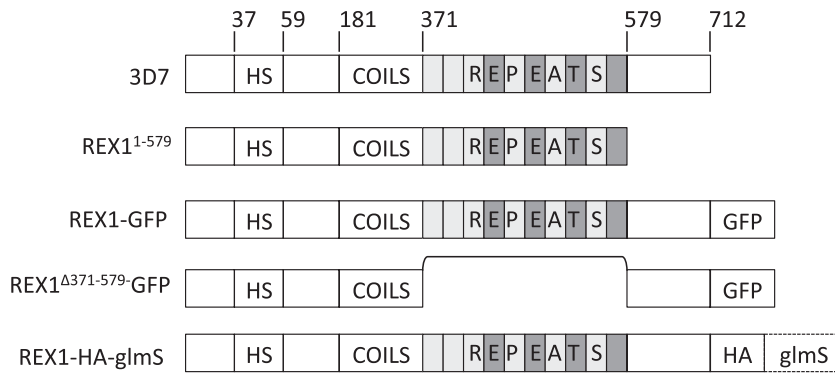


Fig. 1. Schematics of REX1 and REX1 mutants. Full-length 3D7 REX1 features a recessed hydrophobic signal sequence (HS), a predicted coiled-coil region and a repeat region. In REX1¹⁻⁵⁷⁹ transfectants the C-terminal region is deleted. REX1-GFP and REX1^(Δ371-579)-GFP transfectants express REX1 with a C-terminal GFP tag, with and without the repeat region. REX-KD transfectants have a 3xHA tag and *glmS* sequence integration into the 3' untranslated region.

with a diameter of ~ 500 nm and a thickness of ~ 40 nm (Hanssen *et al.*, 2008b). They are connected to the RBC membrane via direct cytoskeletal interactions (Cyrklaff *et al.*, 2011) and via distinct tether-like structures (tubes of about ~ 25 nm by ~ 200 nm) (Hanssen *et al.*, 2010; Pachlatko *et al.*, 2010). The Maurer's clefts are thought to function as a sorting compartment; some exported proteins transiently associate with the Maurer's clefts *en route* to the RBC cytoskeleton or membrane, while some remain as resident proteins. Resident proteins play important roles in the PfEMP1 trafficking process; and proteins such as the ring exported protein-1 (REX1) (Dixon *et al.*, 2011), the skeleton-binding protein-1 (SBP1) (Cooke *et al.*, 2006; Maier *et al.*, 2007), the membrane-associated histidine-rich protein-1 (MAHRP1) (Spycher *et al.*, 2008), PfEMP1 trafficking protein 1 (PfPTP1) (Rug *et al.*, 2014) and *P. falciparum* antigen 332 (Glenister *et al.*, 2009) have been shown to be essential for efficient delivery of PfEMP1 to the RBC surface.

REX1 is a peripheral membrane protein that is exported to the RBC cytoplasm in the very early ring stage of infection (~ 2 h post-invasion) (McMillan *et al.*, 2013), where it associates with a population of already formed Maurer's clefts (Gruring *et al.*, 2012). This 712 amino acid protein possesses a recessed hydrophobic signal sequence (residues 37–58), a predicted coiled-coil region (residues 181–361), a highly charged repetitive sequence region (residues 362–579) and a C-terminal region (residues 580–712) (Fig. 1). It has no predicted *Plasmodium* Export Element (PEXEL) and is thus considered to be a PEXEL-Negative Exported Protein (Spielmann and Gilberger, 2010; Gruring *et al.*, 2012).

Previously, we have shown that attachment of REX1 to the Maurer's clefts is mediated by a sequence within the predicted coiled-coil domain (Dixon *et al.*, 2008). Interestingly, targeted truncation of REX1 leads to an altered Maurer's cleft architecture and a significant decrease in PfEMP1 surface exposure (Hanssen *et al.*, 2008a; Dixon *et al.*, 2011). However, complete genetic disruption of REX1 was found to be associated with concomitant

deletion of the sub-telomeric region of chromosome 2, with resultant loss of the genes for a number of exported proteins, including the knob-associated histidine-rich protein (KAHRP). KAHRP forms the main structural component of the knobs at the infected RBC surface in which PfEMP1 is concentrated (Horrocks *et al.*, 2005) and promotes PfEMP1 presentation (Crabb *et al.*, 1997). This makes it difficult to distinguish the direct effect of REX1 on PfEMP1 trafficking from an indirect effect due to the loss of knobs and other deleted chromosome 2 genes.

In this work, we have used the inducible ribozyme system (Prommana *et al.*, 2013) to genetically attenuate the expression of REX1 and show that Maurer's cleft architecture changes can be achieved, independent of loss of the *kahrp* locus. We have mapped the key domain within REX1 that controls cleft architecture and forward trafficking of PfEMP1. That is, we show that removal of the repeat sequence region (residues 362–579) results in the formation of giant stacked Maurer's clefts. This is associated with significant loss of PfEMP1 surface delivery and decreased adhesion of infected RBCs. Using sophisticated prediction methods, we gain some insights into the physical nature of REX1 and its role in Maurer's clefts sculpting.

Results

Knockdown of REX1 expression is associated with Maurer's cleft reorganization without loss of KAHRP

Genes with important functions in the asexual blood stage are difficult to study using conventional gene disruption strategies due to the haploid nature of the *P. falciparum* genome. Recently, methods have been introduced to target genes by incorporating a glucosamine-6-phosphate – activated ribozyme (*glmS*) into their 3' untranslated region (Fig. S1) (Prommana *et al.*, 2013). In the presence of the cofactor glucosamine-6-phosphate, the *glmS* ribozyme degrades the mRNA encoding the targeted gene thereby reducing its expression.

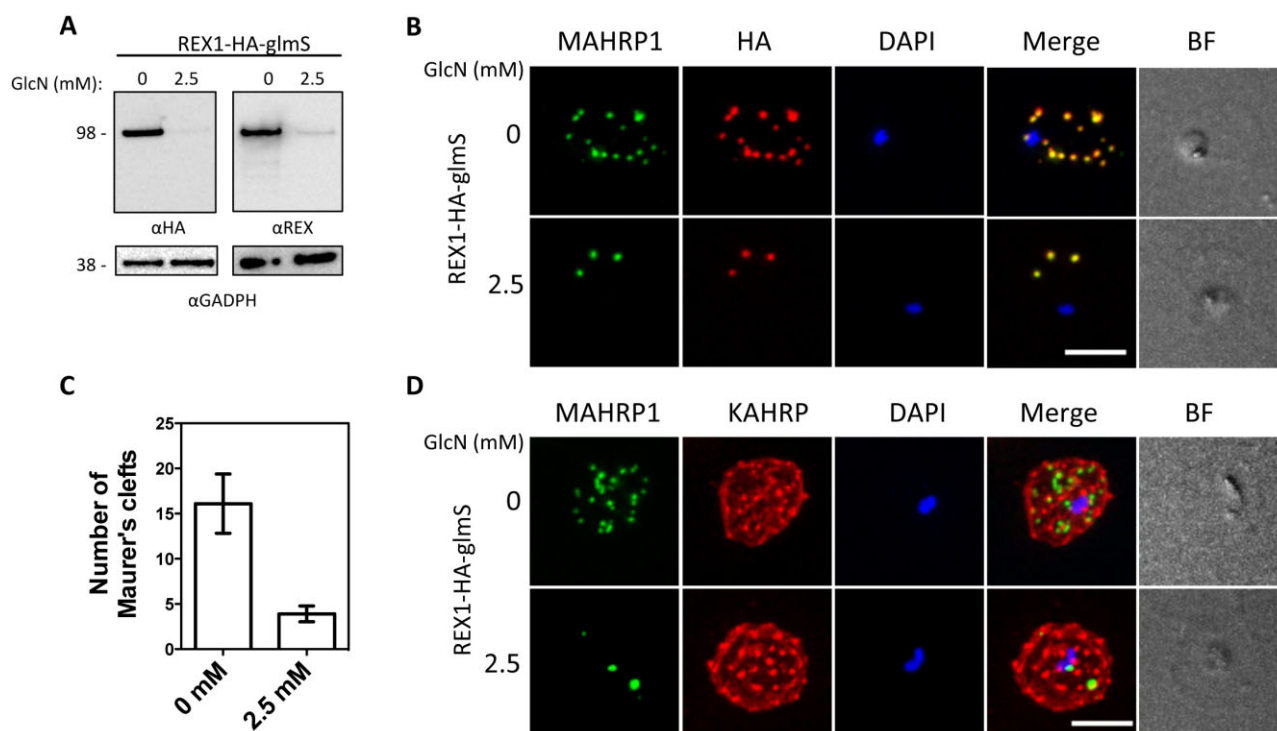


Fig. 2. Inducible knockdown of REX1 using the *glmS* ribozyme system decreases the number of Maurer's cleft puncta.

A. Western blots confirming knockdown of expression of REX1 in REX1-KD transfectants probed with anti-HA and anti-REX1.

B and D. Immunofluorescence microscopy of paraformaldehyde-fixed infected RBCs probed with Maurer's cleft marker anti-MAHRP1 (green) and anti-HA or anti-KAHRP (red). Nuclei are stained with DAPI (blue). Scale bar = 3 μ m.

C. Quantitation of numbers of Maurer's clefts produced by REX1-KD transfectants in the presence and absence of 2.5 mM GlcN. The mean number of Maurer's clefts produced per singly nucleated infected RBC was determined by counting SBP1-labeled puncta in at least 10 cells. Error bars = S.D.

The glucosamine (GlcN)-inducible *glmS* ribozyme and a 3 \times HA tag (Fig. 1) were incorporated into the 3' untranslated region of the REX1 gene by homologous recombination. PCR and DNA sequencing confirmed correct integration of the *glmS* plasmid. Treatment of ring stage REX1-KD parasites with 2.5 mM GlcN (which is converted to glucosamine-6-phosphate) for 20 h, resulted in efficient (> 90%) REX1 knockdown, as quantitated by loss of the HA-tagged REX1 (Fig. 2A). By contrast, the level of a control protein, PfGAPDH, remained unchanged. This indicates that the decline in the REX1 level was not caused by defective or aborted development of parasites. Indeed parasite growth was not affected by the significantly decreased expression of REX1; when monitored over a period of 48 h in the presence of 2.5 mM GlcN, no growth defect was observed in either 3D7 or REX1-KD parasites compared with untreated parasites. Parasitemia levels were 106% of the controls, in both cases (Fig. S2).

Maurer's clefts can be observed by immunofluorescence microscopy following labeling with antibodies recognizing resident proteins such as MAHRP1 and SBP1 (Fig. 2B and D; Fig. S3D). In the absence of GlcN, we

observed 16 ± 3 REX1-HA and SBP1-positive puncta in the REX1-KD parasites (Fig. 2C), which is equivalent to the number found in wild-type 3D7 (see Fig. 3C). These puncta correspond to individual Maurer's cleft cisternae that have a distributed organization within the RBC cytoplasm (Hanssen *et al.*, 2008a).

Upon exposure to 2.5 mM GlcN, the REX1-KD parasites exhibited a decreased number (4 ± 1) of SBP1-positive puncta (Fig. 2C; Fig. S3D) indicating reorganization of Maurer's cleft architecture. Treatment of 3D7 parasites with 2.5 mM GlcN did not affect the number of Maurer's clefts puncta (data not shown). Deletion of the *rex1* gene has been reported to be associated with concomitant disruption of the chromosome 2 locus which contains genes encoding KAHRP and other proteins such as *P. falciparum* Erythrocyte Membrane Protein-3 (PfEMP3) (Dixon *et al.*, 2011). Interestingly, the GlcN-treated REX1-KD parasites retained expression of KAHRP (Fig. 2D) and PfEMP3 (Fig. S3C), indicating that Maurer's cleft restructuring can occur even in the presence of an intact chromosome 2 locus and that reduction of REX1 levels does not affect the trafficking of these proteins to the RBC periphery.

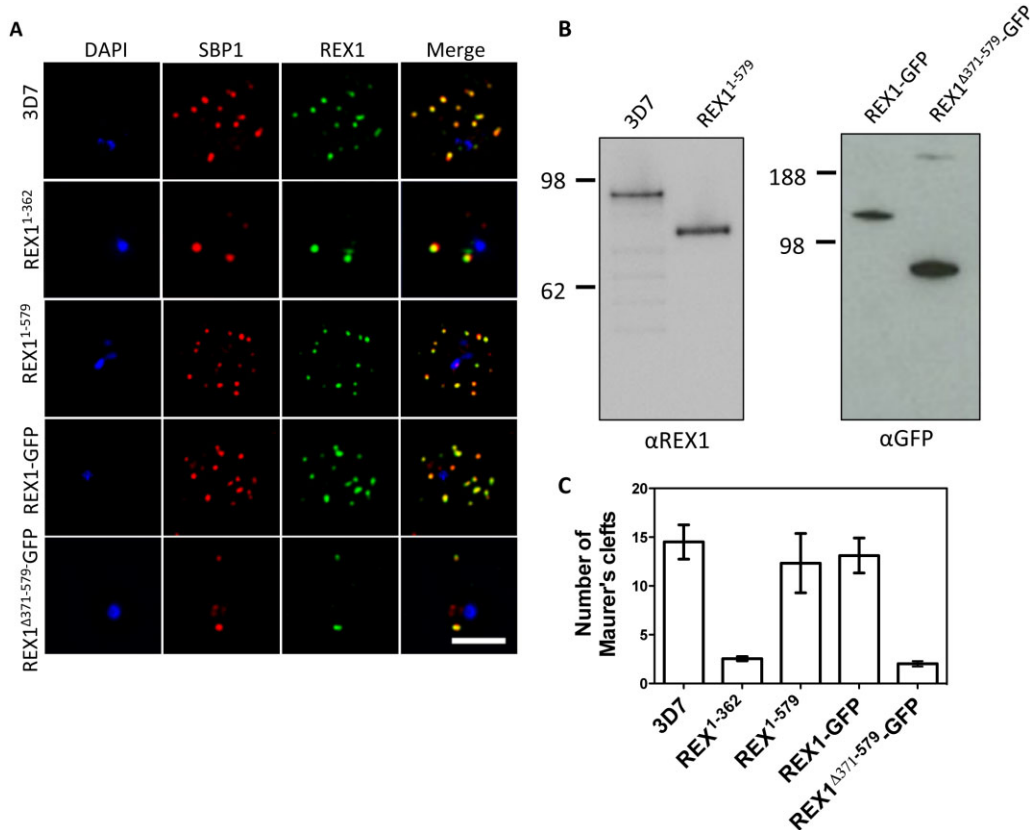


Fig. 3. Deletion of the repeat region of REX1 decreases the number of Maurer's cleft puncta.

A. Immunofluorescence microscopy of acetone-fixed infected RBCs probed with anti-SBP1 (red) and anti-REX1 (green). Nuclei are stained with DAPI (blue). Scale bar = 3 μ m.

B. Western blots confirming expression of REX1 in wild-type 3D7 and truncated REX1¹⁻⁵⁷⁹ (probed with anti-REX1), and REX1-GFP and REX1^(Δ 371-579)-GFP chimeras (probed with anti-GFP).

C. Quantitation of numbers of Maurer's clefts produced by 3D7 and different REX1 transfectants in singly nucleated infected RBCs. Error bars = SD.

The repeat region of REX1 is involved in Maurer's cleft sculpting

In an effort to identify the region within REX1 that is responsible for maintaining normal Maurer's cleft architecture, we targeted the locus to modify the REX1 sequence. We found that removal of the C-terminal half of the REX1 protein, using an integration strategy (REX1¹⁻³⁶²) (see Dixon *et al.*, 2011; Fig. S1), is associated with a dramatic decrease in the number (3 ± 0.2) of SBP1-positive puncta (Fig. 3A and C), similar to that observed with REX1 knock-down parasites. We next generated parasites in which REX1 is truncated at residue 579 (REX1¹⁻⁵⁷⁹; Fig. 1) and used Western analysis to show that a protein of approximately 70 kDa was expressed (Fig. 3B, left panel). These parasites exhibit 12 ± 3 SBP1-labeled puncta (Fig. 3A and C), a Maurer's cleft profile that more closely resembles wild-type 3D7 ($P = 0.54$, unpaired t-test). This indicates that the region between

amino acids 363 and 579 carries the major determinant that controls Maurer's cleft architecture.

To further investigate this, we generated a REX1 construct in which the repeat sequence domain (371-579) was deleted (REX1 ^{Δ 371-579}-GFP; Fig. 1). For this transfectant, we used a GFP-tagged REX1 construct, to facilitate downstream characterization, and compared the mutants with transfectants expressing full-length REX1-GFP and with wild-type 3D7. Western analysis confirms that full-length REX1-GFP migrates with an apparent molecular mass of 120 kDa as expected for the chimera, while the REX1 ^{Δ 371-579}-GFP migrates with the expected molecular mass of 87 kDa (Fig. 3B, right panel).

Immunofluorescence microscopy reveals that full-length REX1-GFP is correctly localized at the Maurer's clefts (Fig. 3A) and that these transfectants exhibit an average number of puncta equivalent to that of the 3D7 parent (13 ± 2 ; $P = 0.59$, unpaired t-test; Fig. 3C). By contrast, the REX1 ^{Δ 371-579}-GFP parasites exhibited a striking Maurer's

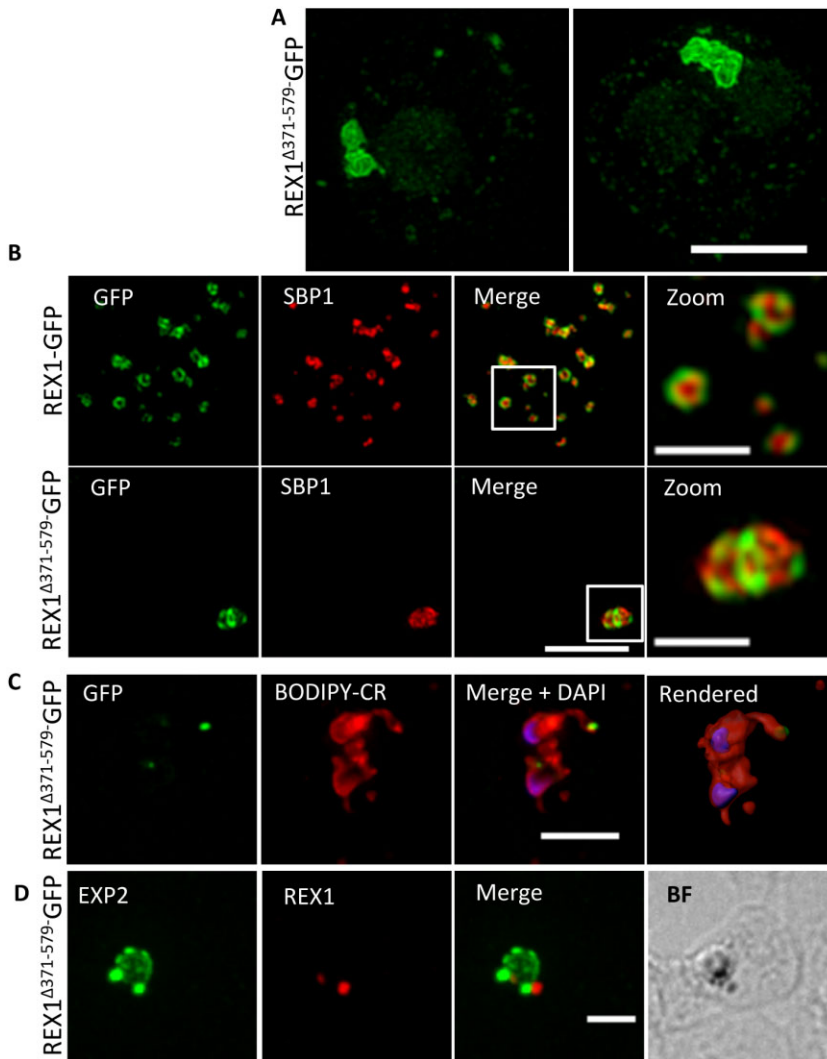


Fig. 4. REX1^{Δ371-579}-GFP parasites exhibit giant Maurer's clefts.

A. REX1^{Δ371-579}-GFP-infected RBCs fixed with paraformaldehyde, permeabilized with EqtlII and labeled with anti-GFP.

B. REX1-GFP and REX1^{Δ371-579}-GFP-infected RBCs were fixed with paraformaldehyde/glutaraldehyde and probed with anti-GFP (green) and anti-SBP1 (red). Samples were examined using 3D-SIM.

C. REX1^{Δ371-579}-GFP-infected RBCs were labeled with BODIPY-ceramide, fixed with paraformaldehyde/glutaraldehyde, labeled with DAPI and imaged using widefield deconvolution microscopy. The right hand panel shows rendering of the surface of the 3D structure using Imaris software.

D. REX1^{Δ371-579}-GFP-infected RBCs were fixed with paraformaldehyde/glutaraldehyde and probed with anti-EXP2 (green) and anti-REX1 (red). Samples were examined using deconvolution microscopy. Scale bars = 3 μm; zoom bar = 1 μm.

cleft phenotype, with only 2 ± 0.3 punctate structures observed in the infected RBC cytoplasm (Fig. 3A and C). This is much less than in wild-type 3D7 and the REX1-GFP line (unpaired t-test, $P < 0.0001$) and even less than the number observed in the REX1 knockdown parasites. These structures were still labeled with SBP1 but appeared larger than the puncta in wild-type parasites.

We performed immunofluorescence microscopy to determine if deletion of the REX1 repeat domain affected the expression or trafficking of other parasite proteins. An anti-KAHRP antiserum gave a roughly homogenous staining pattern at the periphery of RBCs infected with all parasite lines (Fig. S3A). Similarly, a characteristic PfEMP3 profile at the RBC membrane was observed in all parasite lines (Fig. S3B).

Maurer's cleft cisternae have a diameter that is close to the limit of resolution of conventional light microscopy. Therefore, it was not clear whether the decreased number of puncta in the REX1^{Δ371-579}-GFP line was due to a defi-

ciency in generating Maurer's clefts or to the stacking of Maurer's cleft cisternae. We therefore examined these structures using 3D-Structured Illumination Microscopy (SIM), which provides an eightfold increase in volume resolution (Schermele *et al.*, 2008; Hanssen *et al.*, 2010). Infected RBCs were permeabilized with the pore-forming toxin, Equinatoxin II (EqtlII) and labeled with an antibody recognizing GFP (Fig. 4A). 3D-SIM reveals giant Maurer's clefts with an apparently convoluted surface. We also examined the relative organization of REX1^{Δ371-579}-GFP and SBP1 by dual labeled immunofluorescence after fixation and permeabilization (Fig. 4B). A complementary organization of REX1^{Δ371-579}-GFP and SBP1 is evident, consistent with sub-compartmentalization of the Maurer's cleft lamella.

We co-labeled early stage REX1^{Δ371-579}-GFP parasites with the membrane probe, BODIPY-ceramide (Fig. 4C) in an effort to determine the physical organization of the Maurer's clefts relative to the PVM that surrounds the

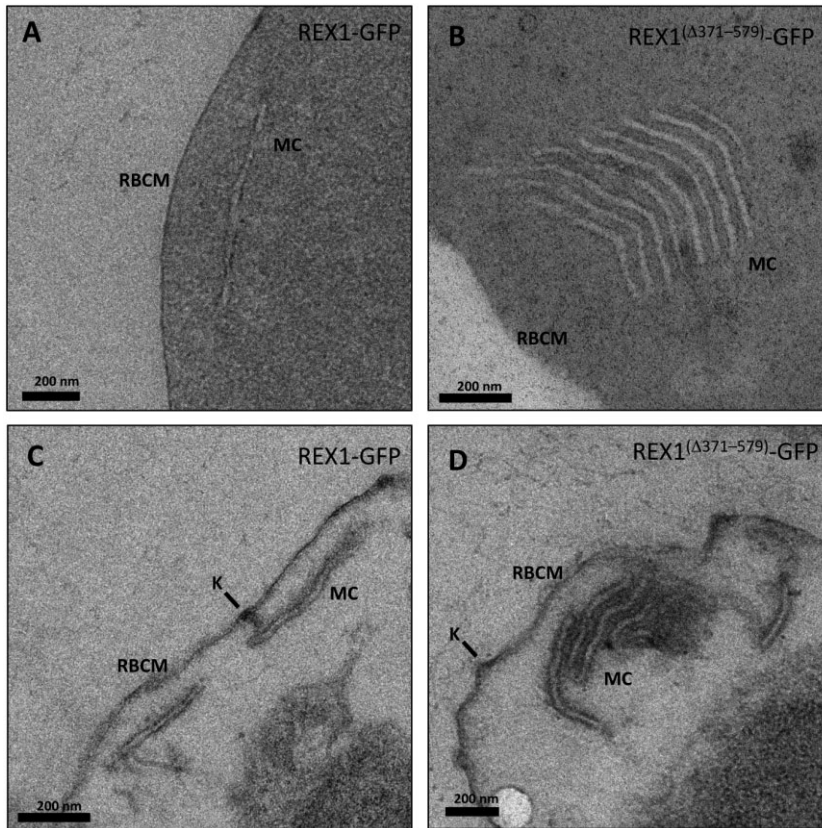


Fig. 5. Transmission electron microscopy analysis of REX1-GFP and REX1^(Δ371-579)-GFP Maurer's clefts.

A and B. TEM images of glutaraldehyde-fixed REX1-GFP and REX1^(Δ371-579)-GFP-infected RBCs (100 nm sections) revealing unstacked and highly stacked Maurer's clefts (MC) lamellae.

C and D. TEM images of EqtII-permeabilized samples showing single Maurer's cleft lamellae and stacked lamellae (100 nm sections). Knobs (K) are indicated.

parasite. The lipid probe BODIPY-ceramide strongly labels membrane structures around the parasite, such as the PVM and the tubovesicular network (Adisa *et al.*, 2003). As observed in this doubly infected ring stage parasite, the REX1^{Δ371-579}-GFP appears to accumulate in discrete puncta close to the PVM. This accumulation is also observed in cells labeled with the PVM marker EXP2 (de Koning-Ward *et al.*, 2009) (Fig. 4D), although the labeling is not overlapping. These puncta may represent nascent Maurer's clefts budding from the PVM or a stack of Maurer's clefts that has become tethered to the PVM.

Transmission electron microscopy was performed to examine further the cleft phenotype in the REX1^{Δ371-579}-GFP parasites. The REX1-GFP parasites displayed an unstacked Maurer's cleft phenotype (Fig. 5A and C) equivalent to that previously reported for the 3D7 strain (Hanssen *et al.*, 2008a). Dramatically, the REX1^{Δ371-579}-GFP parasites showed very large stacks of Maurer's clefts (Fig. 5B). For stacks cut in transverse section, it was possible to estimate the average number of layers in the stack as 6 ± 2 . The average distance between the lamellae was 20 ± 5 nm. The average thickness of the Maurer's cleft lamellae (lumen and both membranes) was 41 ± 8 and 38 ± 8 nm, respectively, for the REX1-GFP and REX1^{Δ371-579}-GFP lines. These data are consistent with

the REX1^{Δ371-579}-GFP parasites producing a similar number of potential cisternae as REX1-GFP parasites but failing to separate them into individual structures.

Tether-like structures accumulate on the stacked Maurer's clefts

In 3D7 parasites, Maurer's clefts are generated soon after invasion (Gruring *et al.*, 2011; McMillan *et al.*, 2013). During the first ~20 h of intraerythrocytic development, Maurer's clefts are often mobile within the RBC cytoplasm (McMillan *et al.*, 2013). They then dock onto the RBC membrane in a process that involves tether-like structures as well as direct interactions with a remodeled RBC membrane skeleton (Cyrklaff *et al.*, 2011; McMillan *et al.*, 2013). To determine the organization of the tether-like structures in REX1^{Δ371-579}-GFP parasites, we made use of a previously described marker of the tethers, the membrane-associated histidine-rich protein-2 (MAHRP2) (Pachlatko *et al.*, 2010). In REX1-GFP parasites, immunofluorescence reveals MAHRP2 labeling (Fig. 6A) closely adjacent to the REX1-GFP labeled Maurer's clefts, as reported previously for wild-type 3D7 (McMillan *et al.*, 2013). For the REX1^{Δ371-579}-GFP parasites, the MAHRP2 labeling partly overlaps with and partly sits outside the single puncta of

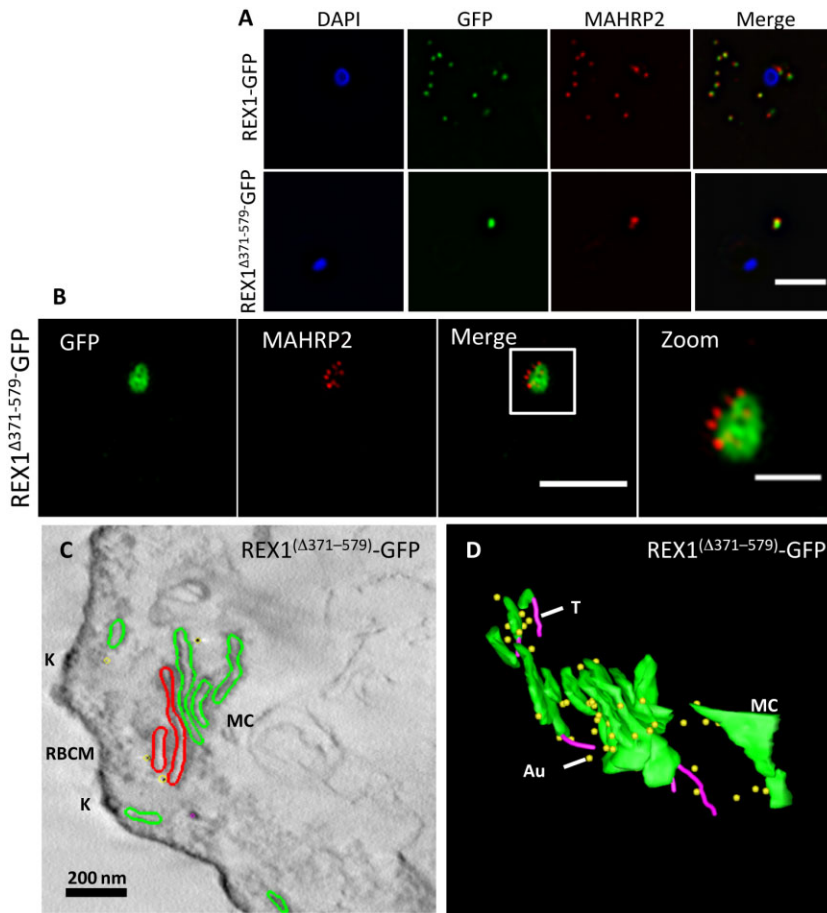


Fig. 6. Analysis of the Maurer's clefts ultrastructure and distribution of tethers of REX1(Δ 371–579)-GFP parasites. REX1-GFP and REX1(Δ 371–579)-GFP transfectants were fixed with paraformaldehyde/glutaraldehyde, permeabilized with Triton X-100 and probed with anti-GFP (green) and anti-MAHRP2 (red). Samples imaged using (A) widefield deconvolution microscopy or (B) 3D-SIM. Scale bars = 3 μ m; zoom bar = 1 μ m. C. STEM tomogram (600 nm section) of an EqtII-permeabilized REX1(Δ 371–579)-GFP-infected RBC showing the stacked Maurer's clefts (MC) layers, and knobs (K) on the RBC membrane (RBCM). The lamella indicated in red share a membrane continuum. D. Rendered STEM tomogram of REX1(Δ 371–579)-GFP-infected RBC labeled with anti-GFP antibodies and protein A gold showing Maurer's clefts (MC, green), tethers (T, magenta) and gold particles (Au, yellow).

GFP labeling. To examine this more closely, we subjected these samples to 3D-SIM (Fig. 6B). This indicates that MAHRP2 is present in small structures that decorate the Maurer's cleft stacks.

To obtain further insights into the Maurer's cleft architecture, REX1 Δ 371–579-GFP transfectants were EqtII-permeabilized, then labeled with anti-GFP and protein A-gold. Sections (600 nm) were prepared for scanning transmission electron microscopy (STEM) tomography (Fig. 6C). Rendering of the different features provides a 3D view of the stacked Maurer's cleft compartments (Fig. 6D). Examination of the STEM tomogram indicated that some of the Maurer's cleft layers are connected by a membrane continuum (Fig. 6C, red), indicating a failure to separate the organelle into individual cisternae. It remains possible that the layered structure is more fully inter-connected in regions that are out of the plane of the STEM tomogram. Protein A-gold-labeled anti-GFP is particularly concentrated on the edges of the REX1 Δ 371–579-GFP Maurer's cleft cisternae, as previously reported for endogenous REX1 (Hanssen *et al.*, 2008b). Several tubular tether structures with a diameter of \sim 25 nm are observed in the reconstructions (rendered in magenta).

The convoluted nature of the Maurer's cleft stack is best appreciated by examining a 3D rotation of the rendered tomogram (Video S1).

It is clear that some of the tether-like structures attached to the Maurer's clefts are not connected through to the RBC membrane; however, given the limited depth of the tomograms, it was difficult to ascertain whether any of the stacked cisternae is directly linked to the RBC membrane. To examine this further, we undertook time-lapse imaging of live REX1-GFP and REX1 Δ 371–579-GFP parasites. As previously reported (McMillan *et al.*, 2013), the REX1-GFP labeled Maurer's clefts are highly mobile during the early to mid-ring stage of parasite development (Video S2; Fig. S4). The majority of Maurer's clefts observed in REX1 Δ 371–579-GFP ring stage-infected RBCs appear to have limited mobility, potentially due to linkage to the parasite surface or trapping in the limited physical space (Video S3; Fig. S4). However, in some REX1 Δ 371–579-GFP cells, the Maurer's clefts are clearly mobile at the ring stage (Video S4; Fig. S4). The Maurer's clefts of both REX1-GFP and REX1 Δ 371–579-GFP immobilize at the trophozoite stage (Fig. S4) consistent with docking onto the RBC membrane.

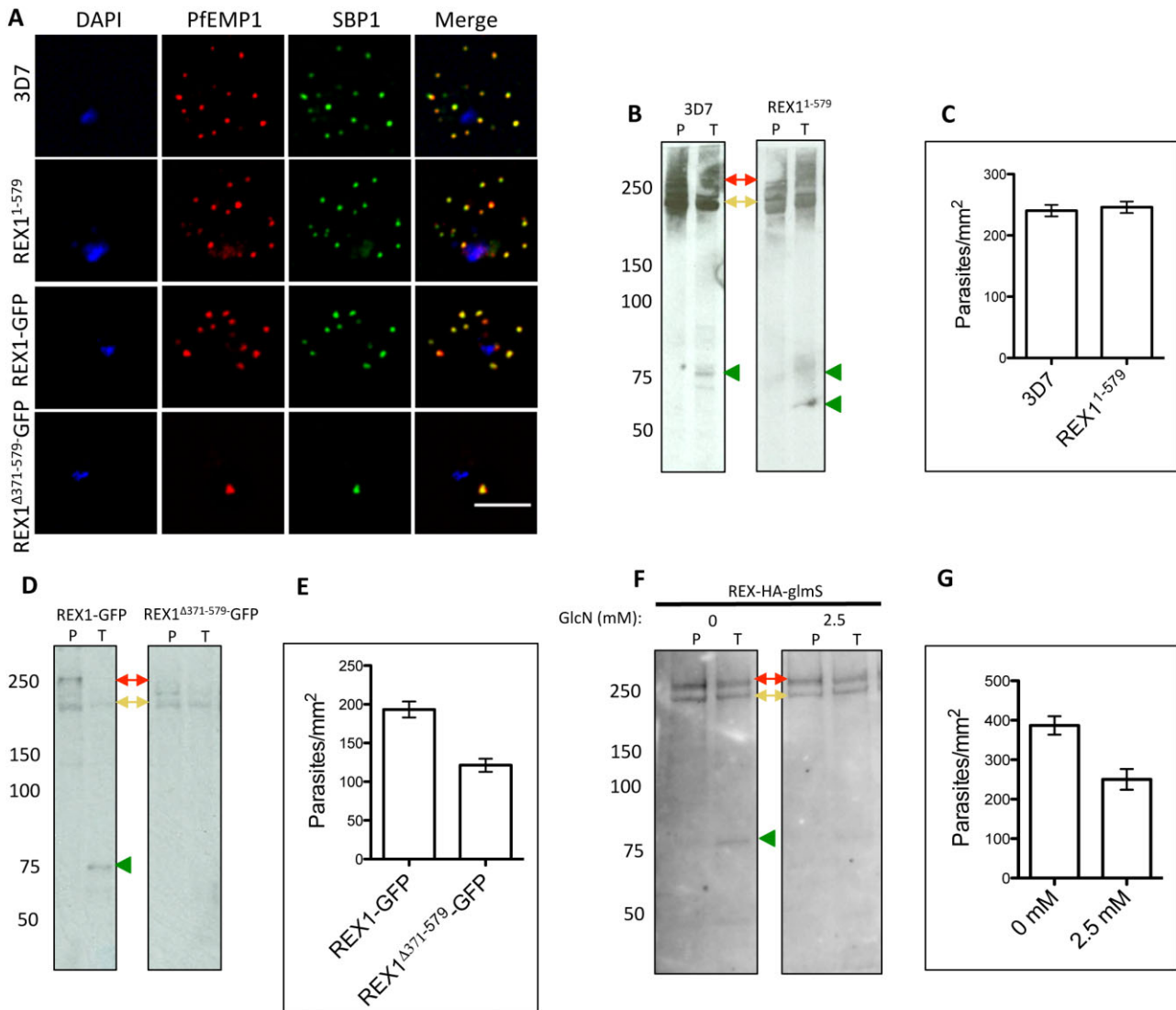


Fig. 7. PfEMP1 surface-exposure and cytoadherence of REX1 transfectants.

A. Immunofluorescence microscopy of acetone-fixed RBCs infected with 3D7 and REX1 transfectants. Maurer's clefts were identified by immunolabeling with anti-SBP1 (green). Anti-PfEMP1 antibodies (red) revealed colocalization of the virulence protein with Maurer's clefts. The nuclei are stained with DAPI (blue). Scale bar = 3 μ m.

B, D and F. Trypsin digestion of surface-exposed PfEMP1 in RBC infected with wild-type and REX1¹⁻⁵⁷⁹ transfectants (B), in REX1-GFP and REX1^(Δ 371-579)-GFP transfectants (D) and in REX1-HA-GlmS parasites without or with treatment with 2.5 mM GlcN. Full-length PfEMP1 (~270 kDa, red arrows) and a cross-reactive spectrin band (~240 kDa, yellow arrows) are indicated. Trypsin cleavage products (75 kDa) are indicated with green arrowheads. The data are representative of three separate experiments.

C, E and G. Adherence of trophozoite-stage infected RBCs to recombinant CD36 under flow conditions (0.1 Pa) \pm S.E.M. measured in 10 different areas in each of three separate experiments. REX1^(Δ 371-579)-GFP binding was significantly lower than REX1-GFP ($P < 0.0001$, unpaired t-test).

The repeat region of REX1 is needed for efficient trafficking of PfEMP1 to the RBC surface

PfEMP1 trafficking requires export into the RBC cytoplasm and transport through the Maurer's cleft intermediate compartment, prior to insertion into the RBC membrane. We examined the organization of PfEMP1 in wild-type 3D7 and REX1 mutant parasites, using immunofluorescence

microscopy on acetone-fixed cells. In agreement with previous studies (Blisnick *et al.*, 2000; Wickham *et al.*, 2001), we observed accumulation of PfEMP1 at the Maurer's clefts in the 3D7 wild-type parasites, as confirmed by co-labeling with the Maurer's cleft marker, SBP1 (Fig. 7A). PfEMP1 is also delivered to the Maurer's clefts in the REX1¹⁻⁵⁷⁹, REX1-GFP and REX1^(Δ 371-579)-GFP mutant parasite lines (Fig. 7A) and in the REX-KD parasites (Fig. S3D).

Thus, despite the aberrant morphology, there is no obvious defect in trafficking of PfEMP1 from the parasite to the stacked Maurer's clefts.

Only a subpopulation of PfEMP1 is delivered to the infected RBC surface (Waterkeyn *et al.*, 2000). This pool of PfEMP1 is oriented with its N-terminal domain exposed at the surface and is thus accessible to cleavage with trypsin (Gardner *et al.*, 1996; Waterkeyn *et al.*, 2000; Kriek *et al.*, 2003). By contrast, intracellular pools of PfEMP1 are protected from protease cleavage. We undertook an analysis of the trypsin accessibility of PfEMP1 in RBCs infected with the different parasite lines. Intact magnet-purified mature stage-infected RBCs were subjected to treatment with PBS (P) or trypsin (T). The Triton-insoluble, SDS-soluble material (representing surface-exposed PfEMP1) was collected and subjected to SDS-PAGE and probed with an antibody recognizing the acidic terminal segment (ATS) domain of PfEMP1. Full-length PfEMP1 from 3D7 parasites migrates with an apparent molecular mass of ~ 270 kDa (Fig. 7B, D and F, red arrows). A cross-reaction of the PfEMP1 antibody with RBC spectrin (at ~ 250 kDa) is observed in variable intensity in the different samples (Fig. 7B, D and F, yellow arrows). Cleavage products of ~ 75 kDa were observed in the trypsin-treated 3D7, REX1-GFP and REX1-KD (no GlcN) samples (green arrowheads). A similar cleavage product was observed in the REX1¹⁻⁵⁷⁹ sample as well as an additional product ~ 60 kDa, likely representing another PfEMP1 variant (Fig. 7B). By contrast, the ~ 75 kDa cleavage products were not detected in the REX1^{Δ371-579}-GFP parasites (Fig. 7D) and was reduced in the REX1-KD parasites treated with 2.5 mM GlcN (Fig. 7F). This suggests a significant reduction of surface-exposed PfEMP1 in these parasites. By contrast, we observed no obvious difference between the level of full-length Triton X-100-insoluble PfEMP1 in the GlcN-treated and control samples (three experiments). To control for the possibility of cell lysis during trypsin treatment, we used SBP1 as a control. There is no evidence for the SBP1 cleavage product that would be expected if the RBC membrane was breached during the trypsin treatment protocol (see Fig. S5).

To assess the functional consequences of the decreased surface-exposed PfEMP1, parasite-infected RBCs were panned on immobilized CD36, to enrich the population for CD36-binding variants of PfEMP1, and then examined for their ability to adhere to immobilized CD36 under flow at a pressure of 0.1 Pa (Fig. 7C, E and G). Because binding levels differ depending on factors such as CD36 batch, it is important to compare matched pairs of samples strictly in parallel. The 3D7 parasites showed no significant difference in binding compared with REX1¹⁻⁵⁷⁹ ($P = 0.68$, unpaired t-test). The REX1^{Δ371-579}-GFP mutants bound significantly less efficiently to CD36 (37% decrease; $P < 0.001$) than REX1-GFP. Similarly,

addition of 2.5 mM GlcN to the REX1-KD parasites significantly decreased the binding to CD36 (35% decrease; $P < 0.001$). This confirms that loss of PfEMP1 surface exposure leads to a significant reduction in adhesion to endothelial ligands. To control for the possibility that treating with GlcN may affect parasite viability, we also measured the CD36 binding of GlcN-treated and untreated 3D7 parent parasites and found no difference (Fig. S6; $P = 0.125$, unpaired t-test).

REX1 is predicted to be highly α -helical

Sophisticated algorithms for predicting protein structure have been developed recently. For example, I-TASSER (Iterative Threading ASSEmblY Refinement) (<http://zhanglab.ccmb.med.umich.edu/I-TASSER/>) uses a multiple-threading program (Local Meta-Threading-Server; LOMETS) to identify related structures from the Protein Data Base (PDB), and then constructs full-length models by iterative template fragment assembly simulations (Zhang, 2008; Roy *et al.*, 2010). The REX1 sequence was analyzed using I-TASSER. The resulting secondary structure prediction indicates largely helical structure throughout the protein (Fig. S7A). Of particular note is the repeat region, which is predicted to be helical throughout, with prediction scores of 9, indicating high confidence. The top model generated for REX1 is presented in Fig. S7B and shows a predominantly α -helical structure. The C-score for this model is outside the range specified for high confidence (Roy *et al.*, 2010), and sequence homology between REX1 and the structure used to construct the model is low (< 10%). Thus, further work is needed to confirm features of this model. Nevertheless, the prediction of helical structure in the repeat region allows some insight into the possible structural properties of this part of the protein. The repeat sequence domain in the 3D7 strain of *P. falciparum* takes the form AAABABABAB, where A and B are variants of PQA EK DASKL TTT YDQ TKEVK and PQA EK DALAKTENQNGELL respectively. Analysis of individual repetitive segments reveals alternating negatively and positively charged regions, with a distinct distribution of charged amino acids in the two repeat types (Fig. S7C). These features will result in a repetitive pattern of charge distribution in this area of the protein. The multiple repeat segments may form extended helices, with the proline residues at the start of each repeat potentially inducing kinks or disrupting the extension of the helix.

Discussion

The virulence of *P. falciparum* is due, in part, to its ability to present PfEMP1 at the RBC surface, which enables sequestration of infected RBCs within the microvasculature of the host. Differences in the severity of malaria-

induced pathologies are thought to arise from the expression of different PfEMP1 variants that bind to different endothelial cell receptors or to the same receptor with different affinities. However, differences in the efficiency of trafficking or presentation of PfEMP1 may also contribute to the adhesion phenotype. For example, alterations in Maurer's cleft architecture may directly or indirectly affect the efficiency of PfEMP1 trafficking to the RBC membrane.

Previous efforts to ablate the *rex1* gene resulted in concomitant loss of a subtelomeric region of chromosome 2, encoding KAHRP and other proteins. Because of the inefficiency of conventional knockout strategies in *P. falciparum*, several months of continuous culturing may be required to retrieve a knockout clone. If a genetic manipulation confers even a small growth disadvantage additional genetic changes may occur that relieve this disadvantage. For example, the loss of the sub-telomeric region of chromosome 2, which encodes several exported proteins that are not needed for survival in culture, is a frequent event during long-term culture.

In this work, we took advantage of a recently developed system for conditional knockdown of *P. falciparum* genes. We achieved > 90% knockdown of REX1 upon addition of GlcN to REX1-KD parasites. This was not associated with a measurable growth defect over the period examined (48 h) but a disadvantage may manifest over a longer period, or upon complete deletion of *rex1*. Maurer's cleft reorganization was observed in these REX1-depleted parasites, confirming its important role in maintaining normal organization. No loss of the chromosome 2 proteins, KAHRP and PfEMP3, was observed, indicating that it is possible to lose REX1 and maintain the expression of these other exported proteins. Nonetheless, REX1-KD mutants showed defective PfEMP1 surface presentation and defective binding under flow. This confirms that REX1 plays a role in PfEMP1 trafficking that is independent of effects on other exported protein. The level of this defect (~ 35% lower binding) was less than that reported for complete *rex1* deletion (Dixon *et al.*, 2011). This likely indicates that the loss of knobs also contributes to the loss of adhesion in this REX1-deleted line but may also reflect the fact that a small amount of REX1 is still expressed in the REX1 knockdown. Contrary to previous reports (Wickham *et al.*, 2001; Knuepfer *et al.*, 2005), we did not observe KAHRP or PfEMP3 colocalizing with Maurer's clefts proteins. This may be due to stage differences or to the fact that these previous studies used truncated constructs of KAHRP and PfEMP3, which may have affected protein localization.

We were interested to further dissect the region of REX1 that is responsible for Maurer's cleft sculpting and effective PfEMP1 trafficking. We showed that deletion of 341 amino acids from the C-terminus causes the formation of Maurer's

er's cleft with an average of 3 stacked cisternae and is associated with less efficient PfEMP1 trafficking, consistent with previous work (Dixon *et al.*, 2011). By contrast deletion of the C-terminal 133 amino acids had no significant effect on Maurer's cleft stacking or PfEMP1 trafficking, indicating that the repeat region (371–579 amino acids) contains important functional motifs.

To further investigate the role of this region, we generated transfectants in which the repeat sequence domain was deleted. These parasites exhibited a phenotype that is even more severe than the REX1^{1–362} transfectants. The Maurer's clefts became highly stacked with an average of six layers per stack. Lateral interactions between the cisternal layers membrane were evident, as well as a membrane continuum between some of the layers. Interestingly in early stage parasites the giant Maurer's clefts were attached to the PVM, which is consistent with the suggestion that Maurer's cleft lamellae are formed from a single focus. The appearance and dimensions of the individual cisternae were similar to that in wild-type parasites, and Maurer's cleft markers such as SBP1 were still trafficked to the stacked clefts and located in distinct sub-compartments, as for wild-type 3D7 (McMillan *et al.*, 2013). The clefts were decorated with multiple 25 nm tether-like structures, indicating that this association still occurs; and they still docked onto the RBC membrane in the mature stage of development. The data suggest that the clefts are formed in a similar manner to wild-type Maurer's clefts but fail to separate into individual cisternae.

It is evident that the repeat region plays an important role (either direct or indirect) in Maurer's cleft sculpting, and it is interesting to consider possible molecular mechanisms. I-TASSER predicts that REX1 comprises extended regions of α -helix. The repeat region (residues 371–579) is highly charged with an excess of negatively charged amino acids, giving it an overall pI of 4.9. The bioinformatics analysis suggests that the repeat sequence is organized as α -helical segments, each with a distinct distribution of charged amino acids. REX1 accumulates at the edges of the Maurer's clefts, and it is possible that the charged α -helical regions generate a high surface charge that repels individual cisternae away from their neighbors. Alternatively, it is possible that the REX1 functions as a severing protein in a similar manner to members of the dynamin family. These proteins have extended α -helices that form helical 'coats' that constrict membranes and promote fission (Low *et al.*, 2009; Morlot *et al.*, 2012). Many *Plasmodium* proteins contain repeat regions, including SBP1, which has degenerate repeats of the sequence QXXQ in the C-terminal domain, with a pI of 4.25. These repeats are predicted by I-TASSER to form random coil (data not shown). However, it remains possible that other *Plasmodium* proteins may contribute to the structure of Maurer's clefts by forming extended helices. It is also

possible that deletion of the REX1 repeats alters the 3D structure of the REX1 protein a way that is deleterious to its function.

The REX1^{Δ371–579} mutants exhibited an intact chromosome 2 locus, a normal distribution of KAHRP and PfEMP3, and normal knob morphology. This suggests that REX1 plays no role in the trafficking of these proteins. Similarly, PfEMP1 appeared to be delivered efficiently to the Maurer's clefts indicating that REX1 is not involved in this transport step. By contrast, the REX1^{Δ371–579} mutants (like the GlcN-treated REX1-KD parasites) showed defective PfEMP1 surface presentation and defective binding under flow. It is possible that the repeat domain directly participates in PfEMP1 trafficking, for example by promoting the budding of PfEMP1-containing vesicles from the Maurer's clefts. Alternatively, deleting the repeat region of REX1 may exert an effect by altering the conformation of the protein. Another possibility is that the stacking of the Maurer's clefts may compromise lateral associations of individual Maurer's cleft cisternae with the RBC membrane that are needed for budding of vesicles or packaging of cargo.

Interestingly, an analysis of the REX1 sequences available in PlasmoDB indicates that the repeat region is polymorphic (in sequence and length) in different *P. falciparum* strains. These differences in repeats do not seem to result in the dramatic change in Maurer's cleft morphology that are observed when this region is deleted. Nonetheless, it is possible that repeat region polymorphisms will affect the efficiency of PfEMP1 trafficking, which could in turn contribute to different levels of cytoadhesion, and thus virulence, of field strains. Further analysis of the role of REX1 in trafficking PfEMP1 may provide ways of interfering with its surface presentation. This could provide an important new strategy to combat this lethal human pathogen.

Experimental procedures

Parasite culture

Plasmodium falciparum parasites were cultured as previously described (Trager and Jensen, 1976). Briefly, parasites (3D7 strain) were cultured in O + RBC (Australian Red Cross Blood Service) at 5% hematocrit, in RPMI-GlutaMAX^(TM)-HEPES (Invitrogen) supplemented with 5% human serum (Australian Red Cross Blood Service) and 0.25% AlbuMAX II (Invitrogen). Synchronization of the ring stages were performed by addition of 5% D-sorbitol (Lambros and Vanderberg, 1979). Mature stage parasite-infected RBCs were purified by magnetic separation (CS columns; Miltenyi Biotec). To maintain knob-positive parasites, cultures were routinely subjected to gelatin flotation (Pasvol *et al.*, 1978). Knockdown of protein expression in parasites containing the *glmS* riboswitch was achieved by addition of 2.5 mM glucosamine to trophozoite-stage parasites in culture.

Plasmid constructs and *P. falciparum* transfection

The genomic region of REX1 corresponding to amino acids 1–579 was PCR-amplified from 3D7 gDNA using the REX1⁵⁷⁹fw (**cctaggtgccaactcgaaactcctgc**) and REX1⁵⁷⁹rv (**atcgatatcttttcagcttgagtaag**) primers (*AvrII* and *Clal* in bold). The resultant PCR products were directionally cloned into pHH1-DEST to get pHH1-REX1^{1–579}. The gene sequence used to generate the REX1^{371–579} parasites was synthesized by GeneScriptTM. This sequence contained *Bam*HI and *Pst*I sites at the 5' and 3' ends of the gene allowing directional cloning into the pEntry-GFP gateway compatible vector (Invitrogen). The pEntry-REX1^{371–579}-GFP vector was recombined with the Gateway compatible Destination vector, pHH1-DEST, to yield the final transfection plasmid pHH1-REX1^{371–579}.

The riboswitch-inducible knockdown construct was made by PCR amplifying the 3' region of REX1 with the REX1-glmS-fw (**ggatcctgccaactcgaaactcctgc**) and REX1-glmS-rv (**ctgcagattaaatcacagaacttctag**) primers (*Bam*HI and *Pst*I in bold). This PCR product was directionally cloned into the pGLMS-HA plasmid (Elsworth *et al.*, 2014) to get the pGLMS-REX1-HA construct. Transfections were performed as previously described (Deutsch *et al.*, 2001).

Fluorescence microscopy

Fluorescence microscopy was performed on either paraformaldehyde/glutaraldehyde (4%/0.0065%) or acetone-fixed thin blood smears as previously described (Spielmann *et al.*, 2006). The following primary antibodies were used: anti-REX1 (rabbit, 1:2000) (Hawthorne *et al.*, 2004), anti-REX1-N-term (mouse, 1:1000) (Hanssen *et al.*, 2008a), anti-GFP (monoclonal antibody, Roche, 1:500), anti-GFP (rabbit, 1:1000) (Humphries *et al.*, 2005), anti-SBP1 (rabbit, 1:2000) (Cooke *et al.*, 2006), anti-MAHRP2 (rabbit, 1:200) (Pachlatko *et al.*, 2010), anti-PfEMP1 ATS (mAb 1B/98-6H1-1, 1:100) (Maier *et al.*, 2007), anti-KAHRP (mouse, 1:200) and anti-PfEMP3 (mouse, 1:200) (Waterkeyn *et al.*, 2000). Nuclei were visualized by addition of DAPI (1 μg ml⁻¹).

Samples were viewed on a DeltaVision DV Elite Restorative Widefield Deconvolution Imaging System (GE Healthcare/Applied Precision) using a 100X objective (1.4NA). Samples were excited by 390, 475, 542 or 632 nm LEDs and imaged using band pass filters at 435, 523, 994 or 676 nm. Images are presented as projections of whole cell z-stacks (taken at intervals of 0.2 μm) unless otherwise stated.

Structured Illumination Microscopy (Schermelleh *et al.*, 2008) was performed on a DeltaVision OMX V4 Blaze (GE Healthcare/Applied Precision). Samples were excited using 488, 568 or 642 nm lasers and imaged using band pass filters at 528, 608 and 683 nm with a 60X objective (1.42 NA). Images were processed using the SoftWorx imaging software (Applied Precision) or ImageJ software (NIH).

Immunoblotting

Trophozoite stage parasites were enriched from culture by magnetic separation or Percoll purification as previously described (Dixon *et al.*, 2011). Purified cells were lysed with 0.03% saponin and fractionated into supernatant and pellet

fractions as previously described (Dixon *et al.*, 2008). Protein samples were adjusted for equal loading, mixed with 6x SDS loading dye and separated on 4–12% Bis-Tris gels (Life Technologies). Gels were transferred to nitrocellulose membranes and blocked for 1 h in 3.5% skim milk in PBS. The following primary antibodies were used in these study: anti-REX1 (rabbit, 1:2000) (Hawthorne *et al.*, 2004), anti-REX1 (mouse, 1:1000) (Hanssen *et al.*, 2008a), anti-GFP (mAb, Roche; 1:500), anti-GFP (rabbit, 1:1000) (Humphries *et al.*, 2005) and anti-GAPDH (rabbit, 1:1000). Anti-mouse or anti-rabbit horseradish peroxidase-conjugated secondary antibodies (1:25000, Promega) were incubated with the membranes for 1 h at room temperature. All membranes were washed three times for 10 min with 0.1% Tween-20 in PBS, following antibody incubations. Washed membranes were incubated with Clarity ECL reagents (Bio-Rad) and visualized on a Las3000 Imager (Fujifilm).

Trypsin cleavage assay

Surface presentation of PfEMP1 was assessed by trypsin cleavage assay as previously described (Dixon *et al.*, 2011). Briefly, purified late stage parasites ($\sim 10^6$ cells) were subjected to treatment with either phosphate-buffered saline (PBS) alone or TPCK-treated trypsin (1 mg ml⁻¹; Sigma), for 1 h at 37°C. The reaction was stopped by addition of soybean trypsin inhibitor. Samples were then lysed and solubilized with 1% Triton X-100 on ice for 20 min and pelleted by centrifugation. The resultant pellet was solubilized in 2% SDS and the proteins separated on 3–8% Tris-acetate gels (Life Technologies) and transferred to nitrocellulose. Membranes were blocked for 1 h in 3.5% skim milk in PBS prior to incubation with anti-PfEMP1 ATS (mAb 1B/98-6H1-1, 1:100) (Maier *et al.*, 2007) antibodies for 2 h at room temperature. To determine if intracellular epitopes are exposed during trypsin treatment, intact infected RBCs were exposed to trypsin, then TPCK-treated. The intact infected RBCs were then lysed with EqII, to release hemoglobin, and the pellets subjected to SDS-PAGE, transferred to nitrocellulose, blocked and probed with anti-SBP1 (BR5) rabbit antibody (1:1000) (Blisnick *et al.*, 2000). Secondary antibodies and detection were performed as described above.

CD36 binding assays and PfEMP1 variant up-selection

Up-selection of parasites on immobilized CD36 was employed prior to binding experiments to maximize surface expression of PfEMP1. Recombinant human CD36 (125 µg ml⁻¹ in PBS) was immobilized on plastic petri dishes (Spycher *et al.*, 2008). Dishes were blocked with 1% BSA in PBS and washed with RPMI-HEPES. Infected RBCs (1% hematocrit, 3% parasitemia) in RPMI-HEPES were added and incubated for 1 h at 37°C. Unbound cells were gently washed from the dish with RPMI-HEPES. Fresh culture media and RBCs were added to the dish and cultures were maintained as described above.

Binding assays under constant flow conditions were performed in culture chambers (iBIDI µ-Slide I) loaded with recombinant human CD36 (125 µg ml⁻¹ in PBS) and incubated overnight at 4°C. Prior to use the chambers were blocked in 1% BSA in PBS for 1 h at 37°C. Binding assays

were performed on trophozoites > 24 h post-invasion, synchronized to a 6–8 h window. Parasites (1% hematocrit, 3% parasitemia) were resuspended in bicarbonate-free RPMI-HEPES and flowed through the chambers at 0.1 Pa using a programmable Harvard Elite 11 Syringe Pump. All assays were performed at 37°C and were visualized on a DeltaVision DV Elite Restorative Widefield Deconvolution Imaging System (Applied Precision) using a 60X objective. Parasites were flowed through the chamber for 5 min, prior to washing chamber for 5 min in bicarbonate-free RPMI-HEPES under constant flow conditions. The number of bound cells per field was counted for 10 randomly chosen fields.

Electron microscopy and immunolabeling

Trophozoite stage parasites were harvested by magnetic purification and fixed in either 2.5% glutaraldehyde, or in paraformaldehyde/glutaraldehyde (2%/0.0075%) for immuno-EM. Labeling was performed by permeabilizing with ~ 40 µg ml⁻¹ Equinatoxin II for 6 min, washing and fixing again with 2% paraformaldehyde. Cells were then washed and incubated with anti-GFP (mAb, Roche; 1:50) in 3% BSA in PBS, washed and incubated with gold-labeled protein A (6 nm Aurion). Cells were embedded in agarose, fixed in 2% OsO₄ for 1 h, washed twice in H₂O and dehydrated in an ethanol series, then acetone, and then infiltrated with Procure epoxy resin for 2 × 12 h at 60°C. Resin was polymerized with BDMA for at least 48 h at 60°C before thin and thick (100 nm and 600 nm) sections were cut. Sections were placed on 100 h copper grids, stained with uranyl acetate and lead citrate and observed on either a Tecnai Spirit (thin sections) or Tecnai F30 (STEM).

Acknowledgements

We thank Courtney Zlatich for technical support, and Dr Megan Dearnley and Dr Aaron Jex, for useful discussions. We thank Prof Brian Cooke (Monash University), Prof Mike Ryan (Monash University), Catherine Braun-Breton (Université Montpellier), Dr Tania de Koning-Ward (Deakin University) and Prof Alan Cowman (Walter & Eliza Hall Institute) for generously providing antibodies. We thank Paul Gilson and Brendan Elsworth (Burnet Institute) for providing the *glmS* plasmid. Microscopy was performed at the Melbourne Advanced Microscopy Facility and the Biological Optical Microscopy Platform, University of Melbourne. This work was supported by grants from the Australian Research Council and the Australian National Health & Medical Research Council. LT is an ARC Australian Professorial Fellow. MDWG is an ARC Future Fellow.

References

- Adisa, A., Rug, M., Klonis, N., Foley, M., Cowman, A.F., and Tilley, L. (2003) The signal sequence of exported protein-1 directs the green fluorescent protein to the parasitophorous vacuole of transfected malaria parasites. *J Biol Chem* **278**: 6532–6542.
- Baruch, D.I., Pasloske, B.L., Singh, H.B., Bi, X., Ma, X.C., Feldman, M., *et al.* (1995) Cloning the *P. falciparum* gene

- encoding PfEMP1, a malarial variant antigen and adherence receptor on the surface of parasitized human erythrocytes. *Cell* **82**: 77–87.
- Beeson, J.G., Reeder, J.C., Rogerson, S.J., and Brown, G.V. (2001) Parasite adhesion and immune evasion in placental malaria. *Trends Parasitol* **17**: 331–337.
- Blisnick, T., Morales Betoulle, M.E., Barale, J., Uzureau, P., Berry, L., Desroses, S., *et al.* (2000) Pfsbp1, a Maurer's cleft *Plasmodium falciparum* protein, is associated with the erythrocyte skeleton. *Mol Biochem Parasitol* **111**: 107–121.
- Cooke, B.M., Buckingham, D.W., Glenister, F.K., Fernandez, K.M., Bannister, L.H., Marti, M., *et al.* (2006) A Maurer's cleft-associated protein is essential for expression of the major malaria virulence antigen on the surface of infected red blood cells. *J Cell Biol* **172**: 899–908.
- Crabb, B.S., Cooke, B.M., Reeder, J.C., Waller, R.F., Caruana, S.R., Davern, K.M., *et al.* (1997) Targeted gene disruption shows that knobs enable malaria-infected red cells to cytoadhere under physiological shear stress. *Cell* **89**: 287–296.
- Cyrklaff, M., Sanchez, C.P., Kilian, N., Bisseye, C., Simporé, J., Frischknecht, F., and Lanzer, M. (2011) Hemoglobins S and C interfere with actin remodeling in *Plasmodium falciparum*-infected erythrocytes. *Science* **334**: 1283–1286.
- Deitsch, K., Driskill, C., and Wellems, T. (2001) Transformation of malaria parasites by the spontaneous uptake and expression of DNA from human erythrocytes. *Nucleic Acids Res* **29**: 850–853.
- Dixon, M.W.A., Hawthorne, P.L., Spielmann, T., Anderson, K.L., Trenholme, K.R., and Gardiner, D.L. (2008) Targeting of the ring exported protein 1 to the Maurer's clefts is mediated by a two-phase process. *Traffic* **9**: 1316–1326.
- Dixon, M.W.A., Kenny, S., McMillan, P.J., Hanssen, E., Trenholme, K.R., Gardiner, D.L., and Tilley, L. (2011) Genetic ablation of a Maurer's cleft protein prevents assembly of the *Plasmodium falciparum* virulence complex. *Mol Microbiol* **81**: 982–993.
- Elsworth, B., Matthews, K., Nie, C.Q., Kalanon, M., Charnaud, S.C., Sanders, P.R., *et al.* (2014) PTEX is an essential nexus for protein export in malaria parasites. *Nature* **511**: 587–591.
- Gardner, J.P., Pinches, R.A., Roberts, D.J., and Newbold, C.I. (1996) Variant antigens and endothelial receptor adhesion in *Plasmodium falciparum*. *Proc Natl Acad Sci USA* **93**: 3503–3508.
- Glenister, F.K., Fernandez, K.M., Kats, L.M., Hanssen, E., Mohandas, N., Coppel, R.L., and Cooke, B.M. (2009) Functional alteration of red blood cells by a megadalton protein of *Plasmodium falciparum*. *Blood* **113**: 919–928.
- Gruring, C., Heiber, A., Kruse, F., Ungefehr, J., Gilberger, T.W., and Spielmann, T. (2011) Development and host cell modifications of *Plasmodium falciparum* blood stages in four dimensions. *Nat Commun* **2**: 165.
- Gruring, C., Heiber, A., Kruse, F., Flemming, S., Franci, G., Colombo, S.F., *et al.* (2012) Uncovering common principles in protein export of malaria parasites. *Cell Host Microbe* **12**: 717–729.
- Hanssen, E., Hawthorne, P., Dixon, M.W., Trenholme, K.R., McMillan, P.J., Spielmann, T., *et al.* (2008a) Targeted mutagenesis of the ring-exported protein-1 of *Plasmodium falciparum* disrupts the architecture of Maurer's cleft organelles. *Mol Microbiol* **69**: 938–953.
- Hanssen, E., Sougrat, R., Frankland, S., Deed, S., Klonis, N., Lippincott-Schwartz, J., and Tilley, L. (2008b) Electron tomography of the Maurer's cleft organelles of *Plasmodium falciparum*-infected erythrocytes reveals novel structural features. *Mol Microbiol* **67**: 703–718.
- Hanssen, E., Carlton, P., Deed, S., Klonis, N., Sedat, J., DeRisi, J., and Tilley, L. (2010) Whole cell imaging reveals novel modular features of the exomembrane system of the malaria parasite, *Plasmodium falciparum*. *Int J Parasitol* **40**: 123–134.
- Hawthorne, P.L., Trenholme, K.R., Skinner-Adams, T.S., Spielmann, T., Fischer, K., Dixon, M.W.A., *et al.* (2004) A novel *Plasmodium falciparum* ring stage protein, REX, is located in Maurer's clefts. *Mol Biochem Parasitol* **136**: 181–189.
- Horrocks, P., Pinches, R.A., Chakravorty, S.J., Papakrivov, J., Christodoulou, Z., Kyes, S.A., *et al.* (2005) PfEMP1 expression is reduced on the surface of knobless *Plasmodium falciparum* infected erythrocytes. *J Cell Sci* **118**: 2507–2518.
- Humphries, A.D., I., Streimann, C., Stojanovski, D., Johnston, A.J., Yano, M., Hoogenraad, N.J., and Ryan, M.T. (2005) Dissection of the mitochondrial import and assembly pathway for human Tom40. *J Biol Chem* **280**: 11535–11543.
- Knuepfer, E., Rug, M., Klonis, N., Tilley, L., and Cowman, A.F. (2005) Trafficking determinants for PfEMP3 export and assembly under the *Plasmodium falciparum*-infected red blood cell membrane. *Mol Microbiol* **58**: 1039–1053.
- de Koning-Ward, T.F., Gilson, P.R., Boddey, J.A., Rug, M., Smith, B.J., Papenfuss, A.T., *et al.* (2009) A newly discovered protein export machine in malaria parasites. *Nature* **459**: 945–949.
- Kriek, N., Tilley, L., Horrocks, P., Pinches, R., Elford, B.C., Ferguson, D.J., *et al.* (2003) Characterization of the pathway for transport of the cytoadherence-mediating protein, PfEMP1, to the host cell surface in malaria parasite-infected erythrocytes. *Mol Microbiol* **50**: 1215–1227.
- Lambros, C., and Vanderberg, J.P. (1979) Synchronization of *Plasmodium falciparum* erythrocytic stages in culture. *J Parasitol* **65**: 418–420.
- Low, H.H., Sachse, C., Amos, L.A., and Lowe, J. (2009) Structure of a bacterial dynamin-like protein lipid tube provides a mechanism for assembly and membrane curving. *Cell* **139**: 1342–1352.
- McMillan, P.J., Millet, C., Batinovic, S., Maiorca, M., Hanssen, E., Kenny, S., *et al.* (2013) Spatial and temporal mapping of the PfEMP1 export pathway in *Plasmodium falciparum*. *Cell Microbiol* **15**: 1401–1418.
- Maier, A.G., Rug, M., O'Neill, M.T., Beeson, J.G., Marti, M., Reeder, J., and Cowman, A.F. (2007) Skeleton-binding protein 1 functions at the parasitophorous vacuole membrane to traffic PfEMP1 to the *Plasmodium falciparum*-infected erythrocyte surface. *Blood* **109**: 1289–1297.
- Maier, A.G., Cooke, B.M., Cowman, A.F., and Tilley, L. (2009) Malaria parasite proteins that remodel the host erythrocyte. *Nat Rev Microbiol* **7**: 341–354.

- Morlot, S., Galli, V., Klein, M., Chiaruttini, N., Manzi, J., Humbert, F., *et al.* (2012) Membrane shape at the edge of the dynamin helix sets location and duration of the fission reaction. *Cell* **151**: 619–629.
- Murray, C.J.L., Rosenfeld, L.C., Lim, S.S., Andrews, K.G., Foreman, K.J., Haring, D., *et al.* (2012) Global malaria mortality between 1980 and 2010: a systematic analysis. *The Lancet* **379**: 413–431.
- Pachlatko, E., Rusch, S., Muller, A., Hemphill, A., Tilley, L., Hanssen, E., and Beck, H.P. (2010) MAHRP2, an exported protein of *Plasmodium falciparum*, is an essential component of Maurer's cleft tethers. *Mol Microbiol* **77**: 1136–1152.
- Pasvol, G., Wilson, R.J., Smalley, M.E., and Brown, J. (1978) Separation of viable schizont-infected red cells of *Plasmodium falciparum* from human blood. *Ann Trop Med Parasitol* **72**: 87–88.
- Prommana, P., Uthaiyibull, C., Wongsombat, C., Kamchonwongpaisan, S., Yuthavong, Y., Knuepfer, E., *et al.* (2013) Inducible knockdown of Plasmodium gene expression using the glmS ribozyme. *PLoS ONE* **8**: e73783.
- Roy, A., Kucukural, A., and Zhang, Y. (2010) I-TASSER: a unified platform for automated protein structure and function prediction. *Nat Protoc* **5**: 725–738.
- Rug, M., Cyrklaff, M., Mikkonen, A., Lemgruber, L., Kuelzer, S., Sanchez, C.P., *et al.* (2014) Export of virulence proteins by malaria-infected erythrocytes involves remodeling of host actin cytoskeleton. *Blood* **124**: 3459–3468.
- Scherf, A., Lopez-Rubio, J.J., and Riviere, L. (2008) Antigenic variation in *Plasmodium falciparum*. *Annu Rev Microbiol* **62**: 445–470.
- Schermelleh, L., Carlton, P.M., Haase, S., Shao, L., Winoto, L., Kner, P., *et al.* (2008) Subdiffraction multicolor imaging of the nuclear periphery with 3D structured illumination microscopy. *Science* **320**: 1332–1336.
- Spielmann, T., and Gilberger, T.W. (2010) Protein export in malaria parasites: do multiple export motifs add up to multiple export pathways? *Trends Parasitol* **26**: 6–10.
- Spielmann, T., Hawthorne, P.L., Dixon, M.W., Hannemann, M., Klotz, K., Kemp, D.J., *et al.* (2006) A cluster of ring stage-specific genes linked to a locus implicated in cytoadherence in *Plasmodium falciparum* codes for PEXEL-negative and PEXEL-positive proteins exported into the host cell. *Mol Biol Cell* **17**: 3613–3624.
- Spycher, C., Rug, M., Pachlatko, E., Hanssen, E., Ferguson, D., Cowman, A.F., *et al.* (2008) The Maurer's cleft protein MAHRP1 is essential for trafficking of PfEMP1 to the surface of *Plasmodium falciparum*-infected erythrocytes. *Mol Microbiol* **68**: 1300–1314.
- Trager, W., and Jensen, J.B. (1976) Human malaria parasites in continuous culture. *Science* **193**: 673–675.
- Turner, L., Lavstsen, T., Berger, S.S., Wang, C.W., Petersen, J.E., Avril, M., *et al.* (2013) Severe malaria is associated with parasite binding to endothelial protein C receptor. *Nature* **498**: 502–505.
- Voigt, S., Hanspal, M., LeRoy, P.J., Zhao, P.S., Oh, S.S., Chishti, A.H., and Liu, S.C. (2000) The cytoadherence ligand *Plasmodium falciparum* erythrocyte membrane protein 1 (PfEMP1) binds to the *P. falciparum* knob-associated histidine-rich protein (KAHRP) by electrostatic interactions. *Mol Biochem Parasitol* **110**: 423–428.
- Waterkeyn, J.G., Wickham, M.E., Davern, K.M., Cooke, B.M., Coppel, R.L., Reeder, J.C., *et al.* (2000) Targeted mutagenesis of *Plasmodium falciparum* erythrocyte membrane protein 3 (PfEMP3) disrupts cytoadherence of malaria-infected red blood cells. *EMBO J* **19**: 2813–2823.
- White, N.J., Pukrittayakamee, S., Hien, T.T., Faiz, M.A., Mokuolu, O.A., and Dondorp, A.M. (2014) Malaria. *Lancet* **383**: 723–725.
- Wickham, M.E., Rug, M., Ralph, S.A., Klonis, N., McFadden, G.I., Tilley, L., and Cowman, A.F. (2001) Trafficking and assembly of the cytoadherence complex in *Plasmodium falciparum*-infected human erythrocytes. *EMBO J* **20**: 5636–5649.
- World Health Organization (2014) *World malaria report 2014*.
- Zhang, Y. (2008) I-TASSER server for protein 3D structure prediction. *BMC Bioinformatics* **9**: 40.

Supporting information

Additional supporting information may be found in the online version of this article at the publisher's web-site.